

## Bose-Fermi mixtures in an optical lattice

K. Sengupta<sup>(1)</sup>, N. Dupuis<sup>(2;3;4)</sup>, and P. Majumdar<sup>(5;6)</sup><sup>(1)</sup> Theoretical Condensed Matter Physics Division and Center for Applied Mathematics and Computational Science Saha Institute of Nuclear Physics, 1/AF Bidhannagar, Kolkata-700064, India.<sup>(2)</sup> Department of Mathematics, Imperial College, 180 Queen's Gate, London SW 7 2AZ, UK.<sup>(3)</sup> Laboratoire de Physique des Solides, Univ. Paris-Sud, CNRS, UMR 8502, F-91405 Orsay Cedex, France.<sup>(4)</sup> LPTMC, CNRS-UMR 7600, Université Pierre et Marie Curie, 75252 Paris Cedex 05, France.<sup>(5)</sup> Cavendish Laboratory, Cambridge University, Madingley Road, Cambridge, CB3 0HE, UK.<sup>(6)</sup> Harish-Chandra Research Institute, Chhatnag Road, Jhansi, Allahabad 211019, India.

We study an atomic Bose-Fermi mixture with unpolarized fermions in an optical lattice. We obtain the Mott ground states of such a system in the limit of deep optical lattice and discuss the effect of quantum fluctuations on these states. We also study the superfluid-insulator transitions of bosons and metal-insulator transition of fermions in such a mixture within a slave-rotor mean-field approximation, and obtain the corresponding phase diagram. We discuss experimental implications of our results.

PACS numbers: 71.10.Fd, 05.30.Jp, 71.30.+h, 73.43.Ng

## I. INTRODUCTION

Recent experiments on ultracold trapped atomic gases have opened a new window onto the phases of quantum matter<sup>1</sup>. A gas of bosonic atoms in an optical or magnetic trap has been reversibly tuned between superfluid (SF) and insulating ground states by varying the strength of a periodic potential produced by standing optical waves<sup>1,2</sup>. This transition has been explained on the basis of the Bose-Hubbard model with on-site repulsive interactions and hopping between nearest neighboring sites of the lattice<sup>3,4,5,6,7</sup>. Further, theoretical studies of bosonic atoms with spin and/or pseudospin have also been undertaken<sup>8,9,10,11</sup>. These studies have revealed a variety of interesting Mott phases and superfluid-insulating transitions in these systems. On the fermionic side, the experimental studies have mainly concentrated on the observation of paired superfluid states<sup>12</sup> and the BCS-BEC crossover in such systems near a Feshbach resonance<sup>13</sup>.

More recently, it has been possible to generate mixtures of fermionic and bosonic atoms in a trap<sup>14,15</sup>. Initially, the main focus of such experimental studies were to generate quantum degenerate Fermi gases, through sympathetic cooling with bosons. However, a host of theoretical studies followed soon, which established such Bose-Fermi mixtures to be interesting physical systems in their own right<sup>16,17,18,19,20</sup>, exhibiting exciting Mott phases in the presence of an optical lattice. In all of these works, the spin of the fermions in the mixture is taken to be frozen out due to the presence of the magnetic trap. However, more recent works reported in Refs. 21 and 22, considered a Bose-Fermi mixture in an optical trap, where the spins of the fermions can be dynamical degrees of freedom<sup>23</sup>. It has been shown in Ref. 21 that the interaction between the bosons and the fermions in such a mixture can enhance the s-wave pairing instability of the fermions.

In this work, we consider a Bose-Fermi mixture in an optical trap and in the presence of an optical lattice and study the Mott phases and the metal/superfluid-insulator transition for the fermions/bosons of such a mixture using a slave-rotor mean-field theory<sup>24</sup>. The motivation for such a study is two-fold. First, it has been shown in Ref. 18 that the Mott phases of Bose-Fermi mixtures in a magnetic trap are interesting in their own right. In the present study, we chart out the Mott phases of the Bose-Fermi mixture in an optical trap, where the Fermion spins are dynamical degrees of freedom, in the deep lattice limit for a wide range of parameters. As expected, we find that the corresponding Mott phases obtained are much richer than their counterparts studied in Ref. 18. Second, the metal/superfluid-insulator transition of the fermions/bosons in such an interacting Bose-Fermi mixture has not been studied before. Here we develop a self-consistent slave-rotor mean-field theory to study such a transition for the Mott phases which do not have density-wave order with broken translational symmetry and use it to obtain at least a qualitative understanding of the effect of interaction between the fermions and the bosons on the metal/superfluid-insulator transition.

In what follows, we shall assume that the atoms are confined using an optical trap so that Fermion spins are not frozen out. We shall, however, ignore the effect of the harmonic trap potential which is a standard approximation used extensively in the literature<sup>25</sup>. The starting point of our study is the Bose-Fermi Hubbard Hamiltonian that has been developed earlier, with similar approximation regarding the trap potential, from underlying microscopic dynamics of the atoms in the presence of

an optical lattice<sup>17</sup>

$$H = H_F + H_B + H_{FB} \quad (1)$$

$$H_F = \sum_i t_{F(B)} c_i^\dagger c_j + h.c. + \sum_i U_{FF} n_i^F n_{i\#}^F \quad (2)$$

$$H_B = \sum_i t_B b_i^\dagger b_j + h.c. + \sum_i U_{BB} n_i^B n_{i\#}^B + \sum_i U_{FB} n_i^F n_i^B \quad (3)$$

$$H_{FB} = U_{FB} \sum_i n_i^F n_i^B \quad (4)$$

Here  $c_i$  is the fermionic destruction operator with spin  $\sigma = \uparrow, \downarrow$  at site  $i$ ,  $b_i$  represents bosonic destruction operator at site  $i$ ,  $n^{F(B)}$  denotes Fermion (Boson) number operators,  $t_{F(B)}$  and  $U_{FF}$  are nearest neighbor hopping matrix elements and chemical potentials for the fermions (bosons),  $U_{BB}$  and  $U_{FF}$  are the on-site Hubbard repulsion for bosons and fermions respectively, and  $U_{FB}$  denotes the relative interaction strength between the bosons and the fermions. In what follows, we shall take the bosons and the fermions to have fixed chemical potentials  $\mu_{F(B)}$  and same on-site repulsion  $U_{BB} = U_{FF} = U$  and consider  $t_{FB} = U$  and  $t_F = t_B$  as parameters which can be freely varied. The justification of this choice is briefly outlined in Sec. II. Further, we shall only deal with case of a square bipartite lattice in this work since this is simplest to realize experimentally.

The organization of the rest of the paper is as follows. In the next section, we identify the Mott phases of Eq. 1. Next, in Sec. III, we introduce the slave rotor formalism and use it within a mean-field approximation to study the metal/superfluid-insulator transition of the Bose-Fermi Hubbard model (Eq. 1). This is followed by a discussion of possible experiments in Sec. IV. A comparison of the Mott-Hubbard phase diagram obtained using the projection operator technique with those obtained from mean-field theories<sup>3,5,6</sup> and standard strong coupling expansions<sup>26</sup> is given in Appendix A.

## II. MOTT PHASES

In this section, we chart out the Mott phases of the Bose-Fermi system. To do this, we first obtain the phases of the system in the Mott limit ( $t_B = t_F = 0$ ) and then obtain fluctuation corrections over these states to  $O(t_{B(F)}^2 = U^2)$ .

Before obtaining the Mott phases for the Bose-Fermi mixture, let us look briefly into the parameters of the Hubbard model (Eq. 1). These can be determined from the microscopic quantities such as the potential depths  $V_{F(B)}$  due to the laser seen by the atoms and their recoil

energies  $E_{F(B)}^R = \hbar^2 k_L^2 = 2m_{F(B)}$  where  $k_L$  is the wave-vector of the laser and  $m_{F(B)}$  are the masses of the fermions (bosons). The potential depth seen by the atoms depend on the detuning of the laser from their natural wavelengths  $\omega_{F(B)}$  of the fermions (bosons). In fact, it can be shown that, the ratio of the lattice potentials seen by the fermions and bosons are<sup>21</sup>

$$\frac{V_F}{V_B} = \frac{4}{4} \frac{\omega_F}{\omega_B} \frac{\omega_B}{\omega_F} \quad (5)$$

where  $\omega_{F(B)} = \omega_L - \omega_{F(B)}$  denote the detunings for the fermions (bosons) and  $\omega_{F(B)}$  are the corresponding natural linewidths. Since the ratio of the natural linewidths is generally close to unity<sup>14,21</sup>, we see that one can tune the ratio of the lattice depths seen by bosons and fermions by varying the detunings.

In terms of these quantities, we have<sup>17</sup>

$$\begin{aligned} t_{B(F)} &= \frac{1}{2} \sqrt{2} \left( \frac{V_{B(F)}}{E_{B(F)}^R} \right)^{1/4} e^{-2 \sqrt{\frac{V_{B(F)}}{E_{B(F)}^R}}} \\ U_{BB(F)} &= \frac{1}{8} \left( \frac{V_{B(F)}}{E_{B(F)}^R} \right)^{1/4} k_L a_{BB(F)} \\ U_{FB} &= \frac{1}{16} \left( \frac{V_{B(F)}}{E_{B(F)}^R} \right)^{1/4} \frac{(1 + m_F/m_B) k_L a_{BF}}{V_F/E_B = E_F} \end{aligned} \quad (6)$$

where  $a_{FF}$ ,  $a_{BB}$ , and  $a_{FB}$  are the s-wave scattering lengths for interaction between two fermions, two bosons and a Fermion and a Boson respectively. These scattering lengths also can be varied either by choosing different species of fermions or bosons or by tuning them using Feshbach resonance. Further, as we have discussed before, by choosing the laser detuning we can also make the fermions and bosons see either similar or very different lattice potentials. Therefore, instead of calculating these parameters from the microscopics, we shall aim to portray a general picture of the Mott phase diagram. Since the experimental possibilities are limitless, for the sake of brevity, we choose  $U_{BB} = U_{FF} = U$  and vary the ratios  $t_{FB} = U$  and  $t_F = t_B$ . It is clear from the above discussions that such a situation can be always achieved in experiments. We shall consider some such specific examples in Sec. IV.

Next, we consider the Bose-Fermi Hubbard Hamiltonian in the Mott limit. In this limit, the on-site states can be represented as  $|n_0^B; n_0^F\rangle$  and the energy is given by

$$\begin{aligned} E |n_0^B; n_0^F\rangle &= E_F |n_0^F\rangle + E_B |n_0^B\rangle + E_{FB} |n_0^B; n_0^F\rangle \\ E_F |n_0^F\rangle &= \frac{0}{F} n_0^F + \frac{1}{2} n_0^F \quad 1^2 \\ E_B |n_0^B\rangle &= \frac{0}{B} n_0^B + \frac{1}{2} n_0^B n_0^B \quad 1 \\ E_{FB} |n_0^B; n_0^F\rangle &= n_0^F n_0^B \end{aligned} \quad (7)$$

where we have scaled all energies by  $U$  and  $\epsilon_{F(B)}^0 = \epsilon_{F(B)} = U$ . It can be seen from Eqs. 7, that two states  $n_0^B; n_0^F = 1$  and  $n_0^B = 1; n_0^F = 0$  are degenerate when

$$(1)(n_0^F = 1; n_0^B = 0) = \epsilon_F = \epsilon_B \quad (8)$$

whereas three states  $n_0^B; n_0^F = 1; n_0^B = 1; n_0^F = 0$  and  $n_0^B = 0; n_0^F = 1$  are degenerate when

$$\begin{aligned} \epsilon_F^0 &= n_0^F + n_0^B = 1 \\ \epsilon_B^0 &= n_0^F + n_0^B = 1 : \end{aligned} \quad (9)$$

The conditions of these degeneracies, of course, depend on our choice of parameters of the model. It is also to be noted that in Eqs. 8 and 9,  $n_0^F$  and  $n_0^B$  in the ground state are themselves functions of  $\mu$ ,  $\lambda$  and  $t$ , and have to be determined by minimizing Eq. 7 subject to the constraint of  $n_0^F$  and  $n_0^B$  being integers.

The ground state phase in the Mott limit ( $t_b = t_f = 0$ ) diagram can be obtained by numerically minimizing the ground state energy (Eq. 7) for integers  $0 \leq n_0^F \leq 2$  and  $n_0^B$ . For the sake of brevity, we carry out the numerical computation for  $\epsilon_B^0 = \epsilon_F^0 = U$  and present the phase diagram as a function of  $\mu$  and  $\lambda$ . The phase diagram for  $\lambda > 0$  is shown in Fig. 1. We find, as expected from the results of Ref. 21, for  $\lambda > 1$ , the fermions and the bosons repel each other out from a given site so that a site is occupied by either a Boson or a Fermion, but not both. Such states were dubbed as "composite" states of bosons/fermions with a correlation hole of fermions/bosons in Ref. 21. However, in the present scenario, the spins of the fermions are dynamical degrees of freedom which leads to richer variety of possible phases, as we discuss below.

As expected from discussions leading to Eq. 8, a large portion of phase diagram has degenerate ground states corresponding to  $n_0^B = 0; n_0^F = 1$  and  $n_0^B = 1; n_0^F = 0$ . Note that in terms of the original fermions, the degeneracy is actually threefold corresponding to states  $|\downarrow; \uparrow; \downarrow\rangle; |\uparrow; \downarrow; \uparrow\rangle$  and  $|\downarrow; \uparrow; \downarrow\rangle$ . This degeneracy is lifted by quantum fluctuations due to the presence of small but finite  $t_f$  and  $t_b$ . This can lead to three different ground states as sketched in Fig. 2: A) an antiferromagnetic state of fermions with no bosons, B) A state of one boson per site and no fermions, and C) A state with fermions and bosons being the nearest neighbors with an antiferromagnetic order for the fermions. The energies of these states can be estimated using a straightforward  $O(t_{B(F)}^2 = U^2)$  perturbation theory and are given by

$$\begin{aligned} E_A &= \frac{N z t_f^2}{U} = \frac{N z t_b^2}{U} - 2 \\ E_B &= \frac{2N z t_b^2}{U} \\ E_C &= \frac{N z t_b^2}{2U} (1 + \lambda^2) \end{aligned} \quad (10)$$

where  $N$  is the total number of sites in the system and  $z$  is the coordination number of each site. Comparing

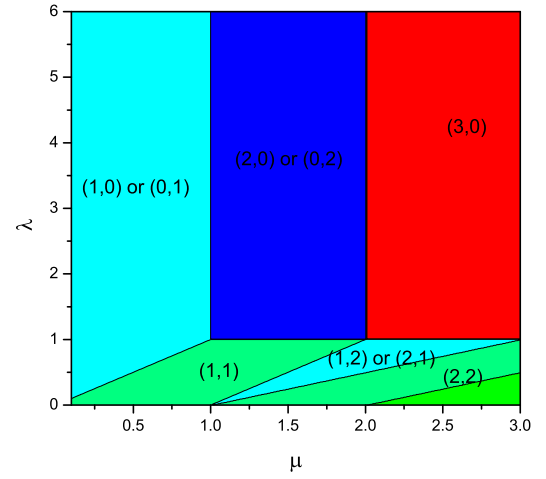


FIG. 1: (Color online) Ground state phase diagram in the atomic limit for  $\epsilon_B^0 = \epsilon_F^0 = U$  and  $\lambda > 0$ . The phases are marked by values of  $(n_0^B; n_0^F)$  in the ground state. For large  $\lambda$ , the system tries to avoid putting bosons and fermions at the same site. The threefold degeneracy between  $(1;0)$  and  $(0;1)$  as well as  $(2;1)$  and  $(1;2)$  occur for a large portion of the phase diagram. In addition, there are doubly degenerate regions such as  $(2;0)$  and  $(0;2)$ . These degeneracies are lifted by virtual hopping process for small but finite  $t_b$  and  $t_f$ .

the energies of the states from Eq. 10, we find that state A is favored over B and C when  $\lambda^2 > 2$  and  $\lambda > (1 + \lambda^2) = 2$ . Similarly the state B is favored for  $\lambda^2 < 2$  and  $\lambda > (1 + \lambda^2) = 4$  and state C for small  $\lambda$  when  $(1 + \lambda^2) = 2 > \text{Max } 2; \lambda^2$ . The corresponding phase diagram is shown in Fig. 2.

With only a nearest-hopping term in the Hamiltonian, the antiferromagnetic ordering in the ground state C is in fact frustrated. Indeed, 4th-order (in  $t$ ) virtual hopping leads to an antiferromagnetic coupling both between next-nearest-neighbor sites and next-next-nearest sites (Fig. 3). In practice, however, this frustration is suppressed by  $O(t^2 = U)$  corrections that arise from the next-nearest neighbor hopping  $t^0$  (not included in the Hamiltonian (2)), leading to an antiferromagnetic order at wavevector  $(\pi; 0)$  (or  $(\pi; \pi)$  in a reference frame tilted by  $45^\circ$ ), in two dimensions as shown in Fig. 2. This should be contrasted with the usual  $(\pi; \pi)$  ordering realized either for state A or for the  $(1,1)$  state shown in Fig. 1. Additional hopping amplitudes (e.g. the next-next-nearest-neighbor hopping  $t^{00}$ ) are expected to be smaller and will not affect the antiferromagnetic ordering of the ground state C. A similar consideration applies for the degenerate states  $(2;1)$  and  $(1;2)$  where quantum fluctuations will similarly lift the degeneracies. Notice that the possibilities of having a ferromagnetic state of fermions where all sites are uniformly occupied

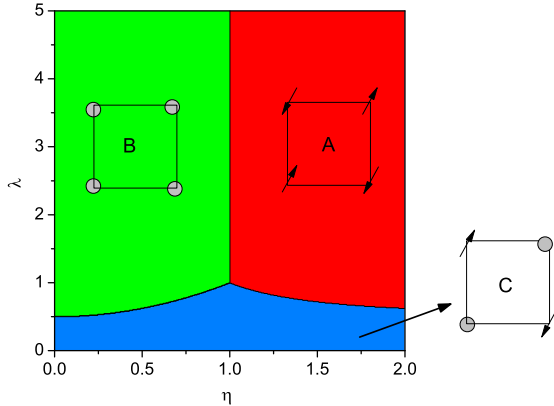


FIG. 2: (Color online) Possible ground states A, B and C that results from lifting the classical degeneracy of the ground states  $(n_0^B; n_0^F) = (1;0)$  and  $(0;1)$  due to quantum fluctuations. Notice that the antiferromagnetic ordering of state C is different from state A and is a consequence of very weak next nearest neighbor hopping. Similar states will result when the degeneracy of the states  $(2;1)$  and  $(1;2)$  is lifted.

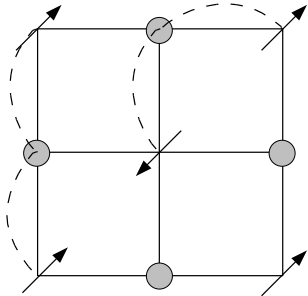


FIG. 3: Virtual hopping (dashed lines) leading to frustration of the antiferromagnetic ground state C. This frustration is lifted and an antiferromagnetic ground state stabilized by virtual hopping generated by the kinetic coupling  $t^0$  between next-nearest neighbor sites (located at opposite corners of the square lattice unit cell).

by  $n$  or  $\#$  fermions never occur since such a state necessarily suppresses Fermion hopping due to Pauli principle and is thus higher in energy compared to the state A.

Finally, we point out that lifting of degeneracy by quantum fluctuations also occurs for the twofold degenerate states labeled as  $(2;0)$  or  $(0;2)$ . Note that the state  $(2;0)$  corresponding to two fermions per site requires that all second order virtual hopping processes are suppressed, unless higher bands are involved. Hence such a state is energetically unfavorable and is never realized. The two other states are D) a homogeneous state with two bosons per site and E) a state with alternate arrangements of two bosons and two fermions per site. The energies of these states are given by  $E_D = 6N z_{\text{B}}^2 U$  and  $E_E = N z_{\text{B}}^2 (1 + \lambda^2) = (2 - 1)U$ . The latter state

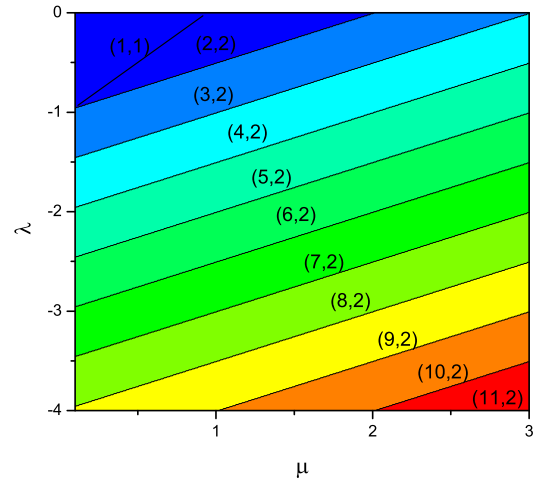


FIG. 4: (Color online) Ground state phase diagram in the Mott limit for  $\lambda < 0$ . The number of fermions per site is  $n_0^F = 2$  while the number of bosons per site is shown in each phase for large negative  $\mu$ .

(E) is thus favored over state (D) for  $\lambda^2 > 6(2 - 1) - 1$ .

In contrast for  $\lambda < 0$  (i.e.  $U_{\text{BF}} < 0$ ), there are no degeneracies. The  $(1;1)$  state persists at all negative  $\mu$ . For  $j > 1$ , the system always has two fermions per site with  $n_0$  bosons, where  $n_0$  is the integer which minimizes  $E[n_0] = n_0 + n_0(n_0 - 1) = 2 - 2j j_0$ . The phase diagram is shown in Fig. 4 as a function of  $\mu$  and  $\lambda$ . The phase diagram corresponds to Mott phase of bosons coupled with non dynamical fixed number of fermions. Note that analogous composite states with  $n_0$  bosons and one Fermion were found and dubbed as "composite Fermion" states in Ref. 21. Here we have almost identical states at large negative  $\mu$  with the difference that there are two fermions per site (instead of one per site as in Ref. 21) owing to the fact that Fermion spins are not frozen in the present study.

### III. SLAVE ROTOR MEAN FIELD THEORY

In this section, we construct a slave-rotor mean-field theory for the coupled Bose-Fermion problem and use it to study the metal/superconductor-insulator transition in this system. We develop the formalism for the mean-field theory in Sec. IIIA, and discuss the results obtained in Sec. IIIB

### A. Formalism

We begin by implementing the slave rotor formalism<sup>24</sup> in the present context. This key observation behind this formalism is that the fermionic Hubbard Hamiltonian (Eq. 2) can be mapped onto a Hamiltonian of free auxiliary Fermions coupled self-consistently to a quantum rotor. The chief advantage of this representation is that the quartic interaction term of the original fermionic Hubbard model can now be represented by a quadratic term in the rotor variables and can thus be treated exactly in the Mott limit. This feature makes this technique suitable for studying Hubbard models in the strong-coupling regime. Further, as shown in Ref. 24, the metal-insulator transition of the original Fermions can be looked upon as the order-disorder transition of the rotors which facilitates the study of metal-insulator transition.

To begin with, we note the identity

$$\frac{1}{2} \sum_i^{\#_2} n_i^F = \frac{1}{2} \sum_i^{\#_2} n_i^F n_i^{\#} = \frac{1}{2} \sum_i^{\#_2} n_i^F + \frac{1}{2} \sum_i^{\#_2} n_i^{\#} \quad (11)$$

so that, up to a constant term, one can write Eq. 2 as

$$H_F = \sum_{\langle ij \rangle} t_{ij}^y c_i^\dagger c_j + h \sum_i^{\#_2} n_i^F + \frac{U}{2} \sum_i^{\#_2} n_i^F + \frac{U}{2} \sum_i^{\#_2} n_i^{\#} \quad (12)$$

Next, following Ref. 24, we introduce the slave rotor representation for the fermions. The key observation here is that the spectrum of  $H_F$  in the Mott limit depends only on the total Fermion number  $n_i$  which can be represented by eigenvalues of angular momenta of a  $O(2)$  rotor. Thus we write the physical fermion annihilation operator as

$$c_i = f_i \exp(i\theta_i) \quad (13)$$

where  $f_i$  denotes the annihilation operator for the pseudo-fermion and  $\theta_i$  denotes the rotor variable at site  $i$ . The corresponding angular momentum of the rotor is denoted by  $L_i = i\partial_{\theta_i}$ . In this representation, a physical fermion state can be written as a product of the pseudo-fermion state and a rotor state as

$$|j_1; c_2; \dots; c_Q; i_1\rangle = |f_1; f_2; \dots; f_Q; i_1; j\rangle = Q \quad |l_i\rangle \quad (14)$$

Here  $l$  denotes the eigenvalues of the rotor angular momentum  $L$  and  $|j_1; c_2; \dots; c_Q; i_1\rangle$  is the antisymmetric combination of Fermionic states for  $Q = 1+1$  fermions at site  $i$ . Note that whereas for ordinary rotors  $l$  can take all possible integer values, here it is constrained to range between  $-1$  and  $1$  by the operator identity

$$L_i = \sum_i^{\#_2} f_i^\dagger f_i = \frac{1}{2} \quad (15)$$

With the following constraint, one can write Eqs. 12 and 4 in terms of the rotor variables as

$$H_F = \sum_{\langle ij \rangle} t_{ij}^y f_i^\dagger f_j \exp[i(\theta_i - \theta_j)] + h \sum_i^{\#_2} n_i^F + \frac{U}{2} \sum_i^{\#_2} n_i^F + \frac{U}{2} \sum_i^{\#_2} L_i^2 \quad (16)$$

$$H_{FB} = U \sum_i^{\#_2} f_i^\dagger f_i n_i^B \quad (17)$$

with  $L_i$  related to  $\sum_i^{\#_2} f_i^\dagger f_i$  by Eq. 15. In the Mott limit ( $t_F; t_B \ll 0$ ), we can implement the constraint (Eq. 15) exactly and this procedure leads to Eq. 7 with  $n_0^F = Q = 1+1$  in a straightforward manner. Note also that the quartic interaction term  $U \sum_i^{\#_2} n_i^F n_i^{\#}$  in Eq. 2 has now been replaced by a quadratic term  $U \sum_i^{\#_2} L_i^2 = 2$  in Eq. 16. This has been done at the expense of generating a non-linear coupling between the auxiliary Fermions and the rotors, as is evident from the first term of Eq. 16.

When  $t_F; t_B \ll 0$ , the above mentioned constraint condition can not be implemented exactly and we need to resort to mean-field approximation. The slave-rotor mean-field theory for the present system can be developed by a straightforward generalization of the formalism developed in Ref. 24. To begin with, we write the system Hamiltonian  $H$  as

$$H = H_r + H_f + H_b \quad (18)$$

$$H_r = \sum_{\langle ij \rangle} t_{ij}^e \cos(\theta_i - \theta_j) + \sum_i^{\#_2} \frac{U}{2} L_i^2 + h L_i \quad (19)$$

$$H_f = \sum_{\langle ij \rangle} t_{ij}^y f_i^\dagger f_j + h \sum_i^{\#_2} n_i^F + \frac{U}{2} \sum_i^{\#_2} n_i^F + \frac{U}{2} \sum_i^{\#_2} n_i^{\#} \quad (20)$$

$$H_b = \sum_{\langle ij \rangle} (t_{ij}^y b_j + h) + \sum_i^{\#_2} \frac{U}{2} n_i^B (n_i^B - 1) + \sum_i^{\#_2} U n_i^F n_i^B \quad (21)$$

where we have implemented the constraint Eq. 15 using an auxiliary field  $h_i$  which has been replaced by its saddle point value  $h$  at the mean-field level. Here we also treat the coupling between the bosons and the fermions within mean-field approximation by replacing the Fermion/bosons density operators  $n_i^{B=F}$  by their averages  $n_{B=F}$ . This amounts to replacing the fermion  $\sum_i^{\#_2} U n_i^F n_i^B$  by  $\sum_i^{\#_2} U n_i^F n_B$  in Eq. 20, and by  $\sum_i^{\#_2} U n_i^B n_F$  in Eq. 21. Within this mean-field approximation, the coupling term acts as a density-dependent shift in the chemical potentials for the bosons and the fermions. The effective hopping matrix elements  $t_{ij}^e$  and

$t_{ij}^e$  in Eqs. 19 and 20 are given by

$$\begin{aligned} t_{ij}^e &= t_{ij} \frac{\hbar \cos(\theta_{ij})}{X} i_{H_r} \\ t_{ij}^e &= t_{ij} \frac{f_i^y f_j^y}{H_f} \end{aligned} \quad (22)$$

with the assumption that averages such as  $\langle \exp(i\theta_{ij}) \rangle$  and  $f_i^y f_j^y$  are real on each bond<sup>24</sup>.

The next step is to approximate the rotor model by an effective single site model

$$H_r^0 = \sum_i K \cos(\theta_i) + \frac{U}{2} L_i^2 + h L_i \quad (23)$$

$$K = \frac{1}{2} \sum_j t_{ij}^e \hbar \cos(\theta_j) i_{H_r} \quad (24)$$

Note that this approximation makes sense only when the Motz ground state does not have density wave order of any kind either for bosons or fermions. Using the fact that under this approximation the  $H_r^0$  becomes a single site Hamiltonian, we define

$$Z = \langle \cos(\theta) \rangle_{H_r^0}^2 \quad (25)$$

and use  $H_f$  to compute all average involving the Fermionic fields. This yields

$$\begin{aligned} K &= 4 \langle \cos(\theta) \rangle_{H_r} \langle n_F \rangle (Z \langle n_F \rangle + h + U n_B) \\ &= 4 \langle \cos(\theta) \rangle_{H_r} \langle n_F \rangle \quad (26) \end{aligned}$$

$$\begin{aligned} h L_i &= 2 \langle n_F \rangle (Z \langle n_F \rangle + U = 2 + h + U n_B) - 1 \\ &= 2 n_F - 1 \quad (27) \end{aligned}$$

where the density of states  $D(\epsilon)$  is defined as  $D(\epsilon) = \int d^3k \delta(\epsilon - \epsilon_k) / (2\pi)^3$ , and  $\epsilon_k = 2t \sum_{i=x,y,z} \cos(k_i)$  is the kinetic energy of the fermions (all momenta are measured in units of lattice spacing), and  $\langle n_F \rangle$  and  $n_F$  are the average fermionic kinetic energy and density respectively. Comparing the expression of  $n_F$  with that for the free fermions  $n_F = \int dD(\epsilon) e^{-\beta(\epsilon - \mu)}$ , where  $\mu$  is the chemical potential for the free fermions at  $T = 0$ , one has the relation

$$Z_0 = \langle n_F \rangle U = 2 + h + U n_B \quad (28)$$

$$h L_i = 2 n_F - 1 \quad (29)$$

Notice that since  $Z$  vanishes at the transition at  $\langle n_F \rangle = \frac{1}{U}$ , one gets  $\langle n_F \rangle U = 2 + h + U n_B$ . Thus  $Z$  acts as the order parameter for the metal-insulator transition of the fermions.

Eqs. 25, 26, 27, 28 and 29 have to be self-consistently solved to obtain the ground state of the system. However, to do this, one needs to obtain the ground state of the bosonic Hamiltonian (Eq. 21) and compute the average value of the boson density  $n_B$ . Since at the mean-field level, the average Fermionic density  $n_F$  enters the boson

Hamiltonian as a shift in the chemical potential, one can use the projection operator technique developed in Ref. 11 for obtaining  $n_B$ . It was shown in the context of two-species Bosons that the projection operator method compares well with quantum Monte Carlo results<sup>11</sup>.

The projection operators for the boson Hamiltonian (Eq. 21) can be constructed following the procedure of Ref. 11. It is given by

$$P_1 = \prod_i n_{0i}^B \prod_j n_{0j}^B \quad (30)$$

where  $n_0^B$  is the Boson occupation per site for the Motz ground state and  $l$  denotes the link connecting two neighboring sites  $i$  and  $j$ .

The hopping term for the bosons can be rewritten in terms of sum over links as

$$T = \sum_l T_l = \sum_l t_b \sum_i b_i^y b_j^y + h.c. \quad (31)$$

where  $i$  and  $j$  are near neighbor sites connecting the link  $l$ . In this notation, one can now divide the hopping term into two parts

$$T_l = T_l^1 + T_l^0 = (P_1 T_l + T_l P_1) + P_1^2 T_l P_1^2 \quad (32)$$

where  $P_1^2 = 1 - P_1$ . It is then easy to see that the term  $T_l^1 = \sum_i T_l^1$  acting on the ground state takes one out of the ground state manifold. The idea is therefore to seek a canonical transformation operator  $S$  which eliminates  $T_l$  to 0 ( $t_b = U$ ) from the low energy effective Hamiltonian:  $[iS; H_0] = -T_l^1$ , where  $H_0$  denotes all the on-site terms in Eq. 4. The effective low energy Hamiltonian can be obtained by the usual Schrieffer-Wolff transformation method

$$\begin{aligned} H &= \exp(iS) H \exp(-iS) \\ &= H_0 + T^0 + [iS; T] + \frac{1}{2} [iS; [iS; H_0]] + \dots \quad (34) \end{aligned}$$

Note that this is equivalent to a systematic  $t_b = U$  expansion and all the omitted terms denoted by ellipsis are at least  $O(t_b^3 = U^3)$ .

The next task is to find out the canonical transformation operator  $S$  in terms of the projection operators  $P_1$ . Following Ref. 11, we guess the form of the  $S$  to be

$$S = i \sum_l [P_1; T_l] \quad (35)$$

where the coefficient  $\alpha$  is to be determined by the condition  $[iS; H_0] = -T_l^1$ . To do this we use the operator identities

$$[P_1 T_l; H_0] = U P_1 T_l; \quad [T_l P_1; H_0] = -U T_l P_1 \quad (36)$$

and evaluate  $[iS; H_0]$  to be

$$[iS; H_0] = \frac{\alpha}{U} \sum_l (P_1 T_l + T_l P_1) = -T_l^1 \frac{\alpha}{U} \quad (37)$$

Thus we find that setting  $\mu = U$  we obtain the expression for  $S = \sum_i [P_i; T_i] = U$ , which eliminates  $T_i$  to 0 ( $t_B = U$ ) from the low energy effective Hamiltonian.

The effective Hamiltonian can be now rewritten by substituting the condition  $[S; H_0] = T^1$  in the last term of Eq. 34 as

$$H = H_0 + T^0 \sum_{\langle l;l' \rangle} [P_l; T_l]; T_{l'}^0 + T_{l'}^1 = 2 \quad (38)$$

With some algebra we now reach the final form of the low energy effective boson Hamiltonian which takes into account all  $t_B^2 = U^2$  fluctuations

$$H = H_0 + T^0 \sum_{\langle l;l' \rangle} \left( \frac{1}{U} \sum_i P_i T_i^2 P_i - T_i P_i T_i + P_i T_i T_{i'} - T_i P_i T_{i'} + \frac{1}{2} P_i T_i T_{i'} P_{i'} - T_i P_i T_{i'} T_{i'} \right) \quad (39)$$

where  $l$  and  $l'$  are nearest neighbor links. One can now use a on-site variational wavefunction in the same way as in Ref. 11

$$\psi = \prod_i \left( a n_0^B |i\rangle + b n_0^B + 1 |i\rangle + c n_0^B |i\rangle \right) \quad (40)$$

to minimize the ground state energy  $E_G = \langle \psi | H | \psi \rangle$  and obtain the corresponding boson density  $n_B$  and superfluid order parameter

$$n_B = \frac{\langle \hat{n}_G^2 \rangle}{q} = \frac{\langle \hat{n}_0^B + 1 \rangle}{q} = \frac{\langle \hat{n}_0^B \rangle}{q} + 1 \quad (41)$$

$$= n_0^B + 1 a_G b_G + n_0^B c_G a_G \quad (42)$$

where  $a_G$ ,  $b_G$  and  $c_G$  are values of the coefficients  $a$ ,  $b$  and  $c$  in the variational ground state. A comparison of the phase diagram obtained by minimizing  $E_G = \langle \psi | H | \psi \rangle$  for  $\mu = 0$  with analogous phase diagrams obtained from mean-field theory<sup>3,5,6</sup> and defect phase calculations to 0 ( $t_B^2 = U^2$ )<sup>26</sup> is presented in App. A.

Eqs. 41 and 42, combined with Eqs. 25, 26, 27, 28 and 29 can now be solved self-consistently to obtain a mean-field description of the coupled Fermi-Bose system near the metal/superfluid-insulator transition points which are signaled by the onset of a non-zero  $Z$  or  $\chi$ . This method, therefore, allows for a self-consistent treatment for the coupled Bose-Fermi problem near the metal/superfluid-insulator transition point, provided that the insulating ground state preserves translational symmetry.

## B. Results

In this section, we discuss the results of application of the formalism developed in the last section to the problem at hand. Here we shall concentrate on the (1;1)

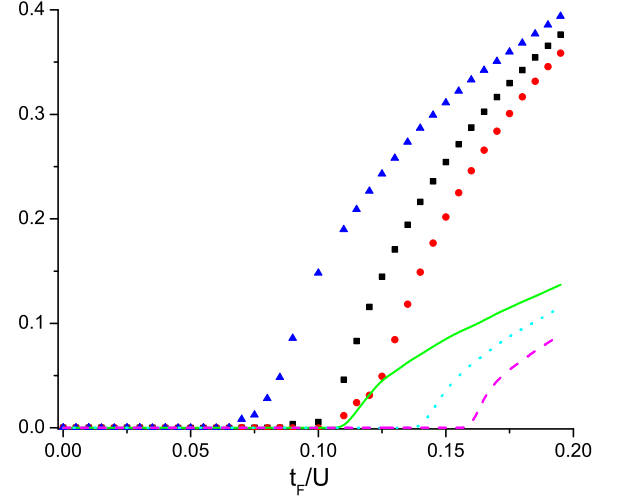


FIG. 5: (Color online) Plot of the order parameter  $\chi$  and  $Z$  for  $\mu = 0.7$  and  $U = 5$ . Non-zero values of  $\chi/Z$  signals superfluid/metal-insulator transition for the Boson/Fermions. The symbols are as follows: black squares and green solid line ( $\chi$  and  $Z$  respectively for  $\mu = 0$ ), red circles and cyan dotted line ( $\chi$  and  $Z$  respectively for  $\mu = 0.3$ ), and blue triangles and magenta dashed line ( $\chi$  and  $Z$  respectively for  $\mu = 0.5$ ).

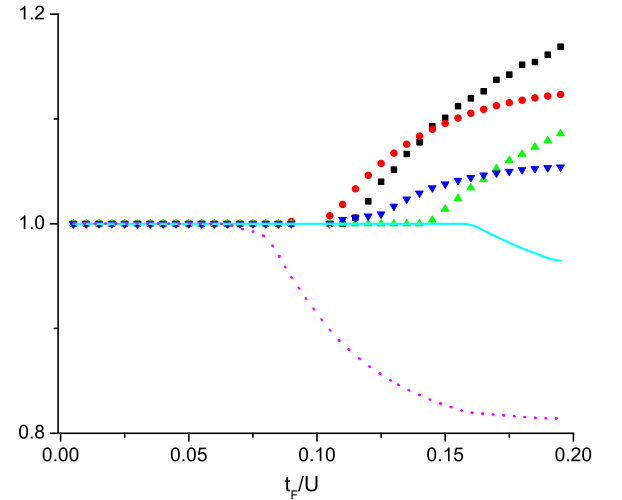


FIG. 6: (Color online) Plot of the average densities  $n_B$  and  $n_F$  for the bosons and Fermions for  $\mu = 0.7$  and  $U = 5$ . The deviation of the densities from their quantized values in the Mott state signals the onset of metal-insulator transition for fermions and superfluid-insulator transition for the bosons. The symbols are as follows: black square and red circle ( $n_B$  and  $n_F$  respectively for  $\mu = 0$ ), green uptriangle and blue downtriangle ( $n_B$  and  $n_F$  respectively for  $\mu = 0.3$ ), magenta dotted line and cyan solid line ( $n_B$  and  $n_F$  respectively for  $\mu = 0.5$ ).

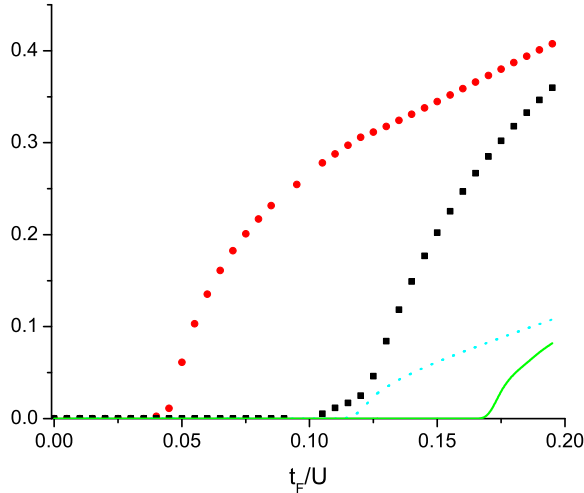


FIG. 7: (Color online) Plot of  $t_F^c$  and  $Z$  for  $\mu/U = 0.4$ ,  $\mu_B = 4$  and  $\mu_F = 0$  and  $\mu = 0.3$ . All symbols have the same meaning as Fig. 5. The plot serves as an illustration that repulsive interaction between bosons and fermions can enhance metal/superfluid transitions.

Mott state for the following reasons. First, since we would be interested in studying metal-insulator transitions for fermions together with the superfluid-insulator transition of bosons, we would like to concentrate on Mott states which has one Fermion per site. Second, in the formalism developed in Sec. IIIA, we treat the Bose-Fermi interaction term within mean-field approximation, we would like to restrict ourselves to the parameter regime  $j_j = j_{FB} = U j < 1$ , where the mean-field results are expected to be more accurate.

To demonstrate the effect of interspecies interaction, we first concentrate on a fixed value of  $\mu_F = \mu_B = 0.7U$  and  $\mu = t_F = t_B = 5$ , and study the onset of metal/superfluid-insulator transition as a function of  $t_F = U$  for a few representative values of  $\mu$ . A plot of  $Z$  and  $t_F^c$  for this case, is shown in Fig. 5 while the fermionic and bosonic densities are plotted in Fig. 6. The results of these plots can be understood as following. Considering  $\mu$  and gradually increasing  $t_F$  so that the fermions/bosons moves towards a metal/superfluid-insulator transition point. As long as the bosons/fermions are in the Mott state, their densities are pinned to  $n_0^B = 1$  or  $n_0^F = 1$ , and hence the fermions/bosons see a fixed chemical potential  $\mu_{F(B)}^e =$

$U n_0^B (n_0^F)$ . For our chosen value of  $\mu$ , the metal-insulator transition occurs before the superfluid-insulator transition of the bosons at  $t_F^c(\mu) = t_F^c(\mu_{F(B)}^e)$ . Notice that  $t_F^c(\mu)$  is a non-monotonic function of  $\mu$  for a given  $\mu$  and  $\mu$ . Hence the metal-insulator transition for the fermions can either be enhanced ( $\mu = 0.5$ ) or hindered ( $\mu = 0.1$ ) due to the Bose-Fermi interaction. Once the fermions have delocalized, the density of fermions changes with  $t_F$

for a fixed chemical potential as seen in Fig. 6. Hence the effective chemical potential seen by the bosons now becomes a function of both  $t_B = t_F = \mu$  and  $\mu$ . Thus by increasing  $t_B$ , we actually traverse a curve with a finite slope in the  $t_B$  plane in contrast to the non-interacting ( $\mu = 0$ ) case. Consequently, the superfluid-insulator transition of the bosons occur at  $t_B^c(\mu)$  which can be quite different from  $t_B^c(\mu = 0)$ . We note this effect may lead to both enhancement [ $t_B^c(\mu) > t_B^c(\mu = 0)$ ] or hindrance [ $t_B^c(\mu) < t_B^c(\mu = 0)$ ] of the superfluid-insulator transition of the bosons depending on the chosen values of  $\mu$  and  $\mu$ , as can be seen by comparing Figs. 5 and 7. For the choice of  $\mu/U = 0.7$  and  $\mu = 5$ , we find that  $t_B^c(\mu) > t_B^c(\mu = 0)$ , whereas the reverse case is realized for  $\mu/U = 0.4$  and  $\mu = 4$ . In the latter case, both the metal-insulator transition for the fermions and the superfluid-insulator transition for the bosons are enhanced for  $\mu > 0$ . Hence we conclude that a repulsive Bose-Fermi interaction can either enhance or hinder the onset of metal/superfluid-insulator transition of a coupled Bose-Fermi mixture held at a fixed chemical potential. Notice that this effect is absent if the boson and the fermion densities are held constant individually, since in that case, there is no influence of the fermionic metal-insulator transition on the bosonic superfluid-insulator transition within the mean-field theory. This is of course an artifact of the present mean-field approximation. Clearly, the dynamics of the fermions/bosons should play an important role in the transition. For example, near the metal-insulator of the fermions, there will be density fluctuations which give the bosons a chance to hop to a neighboring site even if they would remain localized in the absence of such fluctuations. A treatment of this effect requires analysis of the slave-rotor model beyond the present mean-field approximation and is outside the scope of the present study.

Finally, we present a plot of the critical hopping strength  $t_B^c$  in Fig. 8 as a function of  $\mu$  and  $\mu$  for a fixed representative  $\mu/U = 0.7$ . We note that at small  $\mu$ , the superfluid-insulator transition takes place when the fermions are still in the Mott state with their density pinned at  $n_F^0 = 1$ . Consequently, the transition for the boson, within the simple mean-field theory, is the same as that occurring for  $\mu = U$ ;  $t_B^c$  becomes maximum when  $\mu = U/0.4$  or  $0.3$ . However when  $\mu$  is large, the fermions have already undergone the metal-insulator transition when the boson are at their transition point and hence have  $\ln_F i \notin 1$ . Consequently the bosons see a different  $\mu = U \ln_F i$  and hence the value of  $t_B^c$  changes. This is reflected in bending of the phase boundary in the right half of Fig. 8. Analogous plots for  $t_F^c$  will have qualitatively same features.

Before closing this section we would like to make a few qualitative comments. First, the analysis of the phase diagram for negative  $\mu$  with  $j_j < 1$  can be carried out in a similar manner and one obtains qualitatively similar results in this case. Second, at large and negative  $\mu$ , the Mott states correspond to two fermions and  $n_0(\mu)$  bosons localized per site. In this case, with decreasing



## IV. EXPERIMENTS

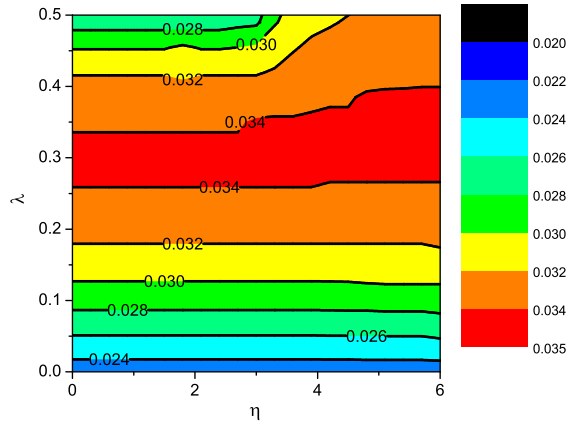


FIG. 8: (Color online) Plot of  $t_F^c/U$  as a function of  $\eta$  and  $\lambda$  for  $\mu/U = 0.7$ . For small  $\lambda$ , the fermions remain in the Mott state when the superfluid-insulator transition of the bosons takes place whereas for large  $\lambda$  they have already undergone a metallic-insulator transition.

lattice potential, the bosons would undergo a superfluid-insulator transition with the fermions still in the Mott phase. Therefore the superfluid-insulator transition of the bosons can be described, within mean-field theory, by a Hubbard model of bosons with effective chemical potential  $\mu_B = \mu - 2U$ . As we decrease the lattice depth, the fermions would eventually delocalize when the hopping coefficient  $t_F$  becomes comparable to the energy gap between the single particle levels ( $E_n \sim 5E_R$ ) in the potential wells. However, this is a large energy scale ( $E_n \sim U; U$ ) for deep lattices and so for any reasonable value of  $\lambda$ , one expects the superfluid-insulator transition of bosons to occur while the fermions are still the Mott state. Third, we would like to note that the slave-rotor mean-field theory worked out here can not be applied for states with broken translational symmetries in terms of boson and fermion numbers (such as the state C shown in Fig. 2) since we have used a single-site approximation for the slave-rotor mean-field theory. Also the present slave-rotor treatment is expected to be more inaccurate for states with  $\lambda > 1$  since the fermion-boson interaction is treated at a mean-field level within our scheme. Nevertheless we note that qualitatively we would expect a Mott-superfluid/metal transition from these phases as  $\lambda$  is reduced keeping the density of bosons and fermions constant. Finally, the present theory can not address the question of possible superconducting instability of the fermions in the metallic state. This issue is discussed in Ref. 21. A generalization of our mean-field description of the superfluid/metal-insulator transitions to address such issues and inclusion of the effect of quantum fluctuations beyond the mean-field treatment used here remain an open problem to be addressed in future works.

A large part of the Mott phases and the superfluid-insulator transition of the Bose-Fermi mixtures discussed here can be experimentally accessed using standard experiments on specific Bose-Fermi mixtures. Before going into details of specific systems, let us first outline some typical experiments that can be performed on these systems. One such experiment that is routinely carried out in atomic systems is measurement of momentum distribution of atoms in the trap<sup>1</sup>. This is typically done in a time-of-flight measurement by letting the atoms fly out by dropping both the lattice and the trap and then measuring the position distribution of the expanding atom cloud. Such a position distribution measurement yields information about momentum distribution of the atoms within the trap. These experiments obtain qualitatively different signatures for atoms in the Mott and the superfluid states for bosons<sup>1,2</sup>, but can not distinguish between the Bose and the Fermi atoms. To achieve this distinction, one needs to pass the expanding atom cloud through a Stern-Gerlach apparatus. Since the fermions and the bosons have different spins (or total angular momenta), they will get separated during this process and can thus be distinguished. Such Stern-Gerlach experiments have been carried out with bosonic atoms in Refs. 27 and 28 and their generalization to present systems should be straightforward. Finally, the antiferromagnetic order of fermions in the Mott phases (either the (1,1) phase in Fig. 1 or the phases A and C shown in Fig. 2) can be determined by measuring spatial noise correlations of the expanding cloud in a time-of-flight measurement<sup>29,30</sup>.

Let us now consider some specific Bose-Fermi mixtures that have been realized experimentally. One such system is <sup>6</sup>Li and <sup>7</sup>Li mixtures with  $a_{FF} = a_{BB} = 5a_0$  and  $a_{BF} > 0$ <sup>31,32</sup>, where  $a_0$  is the Bohr radius. The value of  $a_{BF}$  has not been unambiguously measured in this system, but is expected to be positive indicating a repulsive interaction<sup>31</sup>. For this mixture,  $m_F \neq m_B$  and depending on the value of  $a_{BF}$  and by varying the frequencies of the laser providing the optical lattice (as discussed in Sec. II), we may realize different points on the phase diagram shown in Fig. 1. Of particular interest is the case where  $a_{BF} > a_{FF}$ <sup>21</sup>. In this case, for one atom per site, we expect to obtain one of the Mott phases A, B or C shown in Fig. 2 depending on the specific value of  $a_{BF} = a_{FF}$  and  $t_B = t_F$  which can be varied by slightly changing the ratio  $V_F = V_B$  (Eq. 6)<sup>33</sup>. In this case, one can scan a large part of the phase diagram shown in Fig. 2. The possible antiferromagnetic orders of fermions in phases A or C (Fig. 2) can be determined by measuring the spatial noise correlation measurements<sup>29</sup>. The states B and C can also be distinguished by passing the expanding clouds through a Stern Gerlach apparatus<sup>27,28</sup>. Other possible Mott phases, as shown in Fig. 1, are also possible if there are more than one atom per site. These phases can be detected analogously.

On the other hand, if  $a_{BF} < a_{FF}$ , one may access

the (1;1) phase (Fig. 1) with one fermion and one boson per site. Here in the Mott state, we would find two separate clouds for bosons and fermions in the Stern-Gerlach measurement with an antiferromagnetic state for the fermions which can be deduced in the spatial noise correlation measurement. Further, one can now access the superfluid/metal-insulator transition in this system by reducing the depth of the laser producing the optical lattice. The superfluid-insulator transition can be directly accessed by measuring the momentum distribution of the bosons. This provides us a direct measurement of  $t_B^c$ . One can now also change  $\mu$  as discussed in the last paragraph and access  $t_B^c(\mu)$  for a given  $\mu$ . This would provide access to a line of constant  $\mu$  in the phase diagram of Fig. 8.

Another Fermi-Bose mixture which has been realized so far  $^{40}\text{K}$ - $^{87}\text{Rb}$  mixture<sup>34</sup>. Here one expects  $a_{FF} > 0$ ,  $a_{BB} < 0$  and negative  $a_{FB}$  indicating an attractive interaction between bosons and fermions. The magnitude of  $a_{FB}$  is also measured in Ref. 34 and is found to be around  $3.6a_{FF}$ , although with a large (about 40%) uncertainty. In this system, we expect to find Mott phases where two fermionic atoms sits on the same site with  $n_0$  bosonic atoms. Such states can also be detected in experiments by passing the expanding clouds through a Stern Gerlach apparatus as discussed earlier. The superfluid-insulator transition of the bosons can also be accessed by lowering the lattice depth.

In conclusion, we have studied a Bose-Fermi mixture in an optical lattice trapped by an optical trap. We have sketched a generic phase diagram for the possible Mott states of these systems and also studied the superfluid/metal-insulator transition using a slave-rotor mean-field theory. We have also discussed definite experiments that can be performed on specific experimentally realized systems that can probe at least part of the above-mentioned phase diagrams.

PM's visit to the Cavendish Lab is supported by the EPSRC (UK) and by a Visiting Scholars Grant from Trinity College.

#### APPENDIX A: COMPARISON OF PHASE DIAGRAMS

In this section, we compare the phase diagram for a single species Mott-Hubbard system obtained using the projection operator with those obtained using mean-field theories<sup>3,5,6</sup> and strong-coupling expansions<sup>26</sup>. To do this, we consider the case of zero coupling between the bosons and fermions ( $\mu = 0$ ). Our starting point is the Bose-Hubbard Hamiltonian of Eq. 21 with  $\mu = 0$ . By tracing the same set of steps, as in Sec. IIIA, we then obtain the effective Hamiltonian  $H_{\text{eff}}$  (Eq. 38). The next step is to obtain the variational energy using the wavefunction  $\psi_{\text{v}}$  (Eq. 40). For the purpose of variational energy computations, it is sufficient to consider  $\psi_{\text{v}}$  with real coefficients  $a, b$  and  $c$  (Eq. 40). This amounts to set-

ting the phase of the superfluid order parameter (Eq. 42) to zero and does not affect the variational energy. A straightforward calculation then yields

$$E_{\text{v}} = \langle \psi_{\text{v}} | H | \psi_{\text{v}} \rangle = E_0 + E_1 + E_2 \quad (\text{A } 1)$$

$$E_0 = E_{\text{p}} b^2 + E_{\text{h}} c^2 \quad (\text{A } 2)$$

$$E_1 = z t_B a^2 (n_0 + 1) b^2 + n_0 c^2 \quad (\text{A } 3)$$

$$E_2 = \frac{z t_B^2 n_0 (n_0 + 1)}{U} a^4 - 2 b^2 c^2 - \frac{z(z-1) t_B^2 n_0 (n_0 + 1)}{U} a^4 (b^2 + c^2) - 4 a^2 b^2 c^2 + \frac{2z(z-1) t_B^2 n_0 + 1}{U} 2bc b^2 (n_0 + 1) + c^2 n_0 - (2n_0 + 1) b^2 c^2 a^2 \quad (\text{A } 4)$$

where  $E_{\text{p}} = (z + U n_0)$  and  $E_{\text{h}} = (z - U (n_0 - 1))$  are the on-site energy costs of adding a particle and a hole respectively to the Mott phase, and  $z = 2d$  denotes the coordination number for a  $d$ -dimensional hypercubic lattice. The phase diagram can now be obtained by minimizing the variational energy  $E_{\text{v}}$  for given  $(t_B = U; \mu = U)$ . The Mott-superfluid phase boundary then corresponds to the minimum value of  $t_c(\mu)$  for which the superfluid order parameter (Eq. 42) is non-zero. Notice that ignoring the  $O(t_B^2 = U^2)$  terms amount to setting  $E_2 = 0$ . Our numerical results in this section, however, retains all terms in  $E_2$ .

Next, we obtain the expression of  $t_c^{\text{mf}}$  using mean-field theory. This can be done in a standard manner as shown in Refs. 3,5,6,37 and the mean-field critical hopping strength in  $d$  dimensions can be obtained<sup>37</sup>

$$t_c^{\text{mf}} = \frac{n_0 + 1}{U n_0} + \frac{n_0}{U (n_0 - 1)} \quad (\text{A } 5)$$

where  $n_0$  denotes the boson occupation number of the Mott phase from which the phase boundary is approached.

Finally, we compare the phase diagram obtained from minimizing the variational energy  $E_{\text{v}}$  with the strong-coupling expansion developed in Ref. 26. The main idea behind the strong-coupling expansion is that at the phase transition point, for a given  $\mu = U$ , the defect state, which corresponds to an additional particle or hole added to the Mott state, becomes energetically more favorable. Thus, the energy difference of the particle or hole defect states with the Mott state given to  $O(t_B^2 = U^2)$  by<sup>35</sup>

$$E_{\text{p}} = E_{\text{p}} - z t_B (n_0 + 1) + \frac{z t_B^2}{2U} (5n_0 + 4) n_0 - \frac{z^2 t_B^2}{U} n_0 (n_0 + 1) \quad (\text{A } 6)$$

$$E_{\text{h}} = E_{\text{h}} - z t_B n_0 + \frac{z t_B^2}{2U} (5n_0 + 1) (n_0 + 1) - \frac{z^2 t_B^2}{U} n_0 (n_0 + 1) \quad (\text{A } 7)$$

vanishes at  $t_B = t_c^h \text{ort}_c^h$ . The phase boundary is obtained by finding the critical hopping  $t_c = M$  in  $[t_c^p; t_c^h]$ .

Before resorting to numerical evaluation of the phase diagram from all different techniques, we would like to clarify the following points. First, although both the defect state calculations of Ref. 26 and the projection operator technique outlined here captures some contributions of  $t_B^2 = U^2$  fluctuations, they are not identical to each other. To see this, we consider a second order virtual process for a defect state with one additional particle (hole)  $|j_0 + (-)1_i\rangle |j_0 i_j\rangle |j_0 + (-)2_i j_0 + (-)1_j\rangle |j_0 + (-)2_i j_0 i_j\rangle$ , where  $i$  and  $j$  are nearest neighbor sites on the square lattice. This process, which after summing over all sites, gives  $O(t_B^2 = U^2)$  energy contributions  $E_p = z^2 t_B^2 n_0 (n_0 + 2) = 2U$  for particles and  $E_h = z^2 t_B^2 (n_0^2 - 1) = 2U$  for holes. Note that all the states involved in such a process lie outside the low energy manifold and hence are not captured within the projection operator technique even if states with  $|j_0 - 2\rangle$  are incorporated in the variational wavefunction (Eq. 40). On the other hand, the projection operator technique together with the variational wavefunctions leads to terms in  $E_2$  (Eq. A 4) which involves product of states with one additional particle and hole (terms which involve product of the coefficients  $b$  and  $c$ ). These terms, which become important mostly near the tip of the Mott lobe, are necessarily absent in defect state calculations in Ref. 26 which considers energy lowering due to a single particle or hole added over the Mott state. Thus we find that the best way to compare different approaches is to compare the phase diagrams obtained using them.

Second, if we neglect the  $O(t_B^2 = U^2)$  terms, the saddle point equations for  $b$  and  $c$  can be easily obtained by minimizing the variational energy in Eqs. A 2 and A 3:

$$\begin{aligned} (n_0 + 1) \frac{E_p}{z t_B} b &= 2(n_0 + 1)b^3 + n_0 c^2 b \\ n_0 \frac{E_h}{z t_B} c &= n_0 c^3 + (n_0 + 1)b^2 c \end{aligned} \quad (\text{A } 8)$$

where we have used the constraint  $a^2 + b^2 + c^2 = 1$ . For the Mott phase, the solution to Eq. A 8 is  $b = 0 = c$  and  $a = 1$ . Note that this ensures that the density in the Mott state is pinned to  $\langle n_i \rangle = n_0$ . Solutions with non-zero  $b$  and  $c$  occurs when in the SF phase for which  $t_B < t_c$ . We find that in the superfluid phase near the Mott transition line, Eq. A 8 admits the following solutions. For  $\mu = U$   $n_0 = 2(n_0 + 1)$  one gets  $t_c = t_c^h = E_h = z n_0$  and

$$c = \frac{1}{\sqrt{2}} \left( 1 - \frac{t_c^h}{t_B} \right)^{1/2} \quad b = 0; \quad (\text{A } 9)$$

whereas for  $\mu = U$   $n_0 = 2(n_0 + 1)$  one has  $t_c = t_c^p = E_p = z(n_0 + 1)$  and

$$b = \frac{1}{\sqrt{2}} \left( 1 - \frac{t_c^p}{t_B} \right)^{1/2}; \quad c = 0; \quad (\text{A } 10)$$

Eqs. A 9 and A 10 show that near the phase transition  $b; c \ll a$ , which is crucial to our analysis. Further, as normally expected in a second order quantum phase transition, the coefficients  $b$  and  $c$  are continuous across the transition. Next, we discuss inclusion of  $O(t_B^2 = U^2)$  terms. If these terms (Eq. A 4) are included, obtaining analytical solutions for  $b$  and  $c$  becomes difficult as it amounts to solving two coupled cubic equations. However, we have checked during numerical evaluation of the phase diagram minimizing Eq. A 1 (which retains second order terms in Eq. A 4) that  $b$  and  $c$  are always small compared to  $a$  near the phase transition and that near the ends of the Mott lobe their numerical values are well reproduced by Eqs. A 9 and A 10.

Finally, we comment about our choice of variational wavefunction in which we have only retained states with one additional particle and hole per site over the parent Mott state. In principle, one can retain states with two or more particle per sites which leads to a more complicated trial wave function. For example, one can retain the states  $|j_0 - 2\rangle$  so that the variational wavefunctions become

$$\begin{aligned} |j\rangle^0_i &= \sum_j |j\rangle^0_i \\ |j\rangle^0_i &= a |j_0 i + 1\rangle + b |j_0 + 1 i + 1\rangle + c |j_0 - 1 i + 1\rangle \\ &\quad + d |j_0 + 2 i + 1\rangle + e |j_0 - 2 i + 1\rangle \end{aligned} \quad (\text{A } 11)$$

which leads to a variational energy to  $O(t_B = U)$  (Eq. 39)  $E_v^0 = \langle H_0 \rangle + T^0 |j\rangle^0_i = E_{0v}^0 + E_{1v}^0$ , where,

$$\begin{aligned} E_{0v}^0 &= E_p b^2 + E_h c^2 + E_{2p} d^2 + E_{2h} e^2 \\ E_{2p} &= 2 + U(2n_0 + 1) \quad E_{2h} = 2 - 3U(n_0 - 1) \\ E_{1v}^0 &= z t_B (n_0 + 1) a^2 b^2 + n_0 a^2 c^2 + (n_0 - 1) c^2 e^2 \\ &\quad + \frac{p}{n_0(n_0 - 1)} c a e + \frac{p}{(n_0 + 2)(n_0 + 1)} b^2 a d \\ &\quad + 2 \frac{p}{(n_0 - 1)(n_0 + 2)} b c d e + (n_0 + 2) d^2 b^2 \\ &\quad + a b c \frac{p}{d n_0(n_0 + 2)} + e \frac{q}{n_0^2 - 1} \end{aligned} \quad (\text{A } 12)$$

To analyze the phase diagram obtained from Eqs. A 11 and A 12, we first note that in the Mott phase  $a = 1$  and  $b = c = d = e = 0$ , as discussed before. Next let us discuss the minimization of  $E_v^0$  near the Mott-SF transition line. When  $d = e = 0$ , the M-I-SF transition occurs at  $z t_c = M$  in  $(t_c^p; t_c^h)$ , with  $b; c \ll 1$  and  $a \approx 1$ . So to find out whether non-zero  $d$  and/or  $e$  is favorable for energy minimization, we need to find the effect of tuning on a non-zero  $d$  and/or  $e$  near this transition point and check whether it leads to lowering of the variational energy. We find that tuning on a non-zero  $d$  and/or  $e$  near this point, as can be seen from the expression of  $E_{1v}^0$  (Eq. A 12), leads to energy gain  $z t_c$  (since in the expression of  $E_{1v}^0$ ,  $d$  and  $e$  always appear as a product with  $b$  and  $c$  which are small), whereas the energy cost (Eq. A 11) is  $O(E_{2p})$  and/or  $O(E_{2h})$ . It turns out that

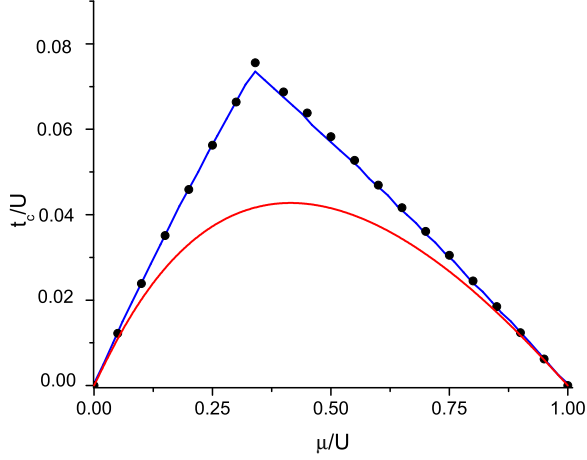


FIG. 9: (Color online) Phase diagram for  $d = 2$  and  $n_0 = 1$  calculated by minimizing variational energy  $E_v$  (black dots), mean-field theory (red solid line) and defect energy calculation to  $O(t_B^2=U^2)$  (blue solid line). The phase boundaries computed by minimizing  $E_v$  and by defect energy calculations compare well to each other but differs from the mean-field theory near the tip of the Mott lobe.

the latter is always greater than the former which leads to a net non-zero energy cost. As a specific example to demonstrate this point, let us consider  $\mu/U$  so that for  $t_B \neq t_c = t_c^c$ ,  $b \neq 0$  and  $c = 0$  (Eq. A10). Then turning on a non-zero  $d$  results in an energy change  $\Delta E = d E_{2p} - d z t_e (n_0 + 2) b^2 d + \frac{d^2}{(n_0 + 2)(n_0 + 1) b^2 a} > 0$  since  $b; d \neq 1$  and  $E_{2h} - z t_e \neq U (n_0 + 1) > 0$ . Thus near  $t_B = t_c$ , the energy cost from  $E_{0v}^0$  clearly outweighs energy gain from  $E_{1v}^0$  (since  $z t_c = U = 1$  for all parameter regime and  $b; c; d; e \neq 1$  near  $t_B = t_c$ ) and hence the coefficients  $d$  and  $e$  remain vanishingly small at the phase transition. As we move inside the superfluid phase and  $t_B$  becomes large compared to  $t_c$ , these coefficients become significant. In the present work, we have always restricted ourselves to regions sufficiently near the transition line where the coefficients  $d$  and  $e$  are small. We note that we have explicitly checked numerically from the full variational energy (including  $O(t_B^2=U^2)$  terms which we have not written down explicitly here to avoid clutter), that the above-mentioned qualitative argument always holds for all the regimes studied in the present work. We shall therefore neglect these terms in the rest of this section.

To compare the results from different approaches, we now plot the phase diagrams for  $n_0 = 1$  obtained by minimizing the full variational energy  $E_v$  to  $O(t_B^2=U^2)$  (Eq. A1), from the mean-field equation (Eq. A5), and by computing the energy of the defect states to  $O(t_B^2=U^2)^{26}$ . These plots are shown in Fig. 9 for  $d = 2$  and in Fig. 10 for  $d = 3$ . We find that in spite of the dissimilarity of the two approaches discussed above, the numeri-

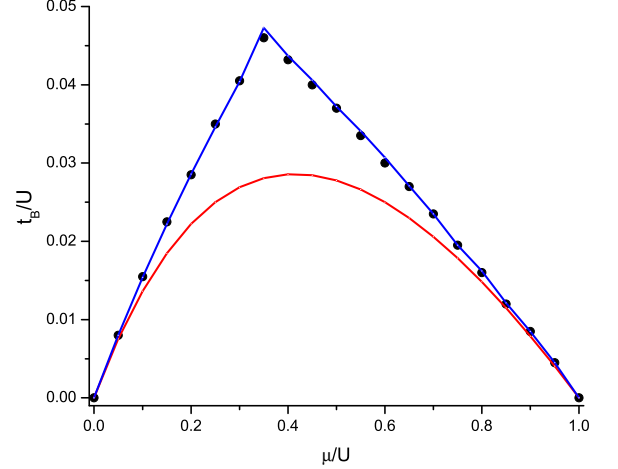


FIG. 10: (Color online) Phase diagram for  $d = 3$  and  $n_0 = 1$ . All notations are same in Fig. 9. As in 2D, the phase boundaries computed by minimizing  $E_v$  and by defect energy calculations compare well to each other but differs from the mean-field theory near the tip of the Mott lobe.

cal phase boundary obtained by minimizing  $E_v$  matches that obtained from  $O(t_B^2=U^2)$  defect state calculation of Ref. 26 quite well in both cases, but differs substantially from the phase boundary obtained using the mean-field theory. Further, for  $d = 2$ , Quantum Monte Carlo data, available for the critical hopping at the tip of the Mott lobe<sup>26,36</sup>, predicts  $(t_c=U)_{MC} = 0.061 \pm 0.006$ . The corresponding values obtained from minimization of  $E_v$  and  $O(t_B^2=U^2)$  defect state energy calculation of Ref. 26 are  $(t_c=U)_{var} = 0.0755$  and  $(t_c=U)_{defect} = 0.0735$  respectively. The mean-field theory predicts a value  $(t_c=U)_{mf} = 0.041$  while an  $O(t_B^3=U^3)$  calculation of defect states energies<sup>26</sup> gives  $(t_c=U)_{defect} = 0.068$ . Thus we conclude that the phase boundary obtained from our variational energy calculation scheme compares well with the defect state energy calculation to  $O(t_B^2=U^2)$ .

In  $d = 3$ , we can compare our results in Fig. 10 to Figs. 5, 6 and 7 for  $\mu/U = 0$  and  $\mu/U = 0.7$  and  $\mu/U = 0.4$  respectively. We find that the phase diagram obtained using the projection operator techniques predicts  $t_c=U = 0.0232$  for  $\mu/U = 0.7$  and  $\mu/U = 5$  (Fig. 5) and predicts  $t_c=U = 0.0431$  for  $\mu/U = 0.4$  and  $\mu/U = 4$ , (Fig. 7). As seen from Fig. 10, these values compare well to those obtained from defect state calculations to  $O(t_B^2=U^2)$ . However, they do not compare favorably with  $t_c^mf=U$  which predicts  $t_c^mf=U = 0.0208$  for  $\mu/U = 0.7$  and  $t_c^mf=U = 0.0266$  for  $\mu/U = 0.4$ . Further, the corresponding values of  $t_c=U$  from the third order defect state calculation are 0.0225 for  $\mu/U = 0.7$  and 0.0405 for  $\mu/U = 0.4$  which compares quite favorably to the projection operator method, but not to the mean-field theory. At the tip of the Mott lobe ( $\mu/U \neq 0.37$ ), where the difference between results obtained from different methods become most appar-

ent, the values of  $t_c=U$  obtained from different methods are 0:0419 (third order defect state), 0:0459 (second order defect state), 0:0451 (projection operator technique),

0:0276 (mean field) and 0:03480(2) (very recently available Quantum Monte Carlo results<sup>38</sup>).

- 
- <sup>1</sup> M . G reiner, O . M andel, T . Esslinger, T W . H ansch, and I . B loch, *Nature* (London) 415, 39 (2002); M . G reiner, O . M andel, T W . H ansch, and I . B loch, *Nature* 419, 51 (2003)
- <sup>2</sup> C . O rzel, A K . T uchman, M L . F enselau, M . Y asuda, and M A . K asevich, *Science* 291, 2386 (2001).
- <sup>3</sup> M . P . A . F isher, P . B . W eichman, G . G rinstein, and D . S . F isher, *Phys. Rev. B* 40, 546 (1989);
- <sup>4</sup> D . J aksch, C . B ruder, J . I . C irac, C . W . G ardinier, and P . Z oller, *Phys. Rev. Lett.* 81, 3108 (1998);
- <sup>5</sup> K . Sheshadri, H . R . K rishnam urthy, R . P andit, and T . V . R am akrishnan, *Europhys. Lett.* 22, 257 (1993)
- <sup>6</sup> D . V an O osten, P . van der Straten, and H . T . C . Stoof, *Phys. Rev. A* 63, 053601 (2001).
- <sup>7</sup> K . S engupta and N . D upuis, *Phys. Rev. A* 71, 033629 (2005).
- <sup>8</sup> A . I m ambekov, M . L ukin, and E . D em ler, *Phys. Rev. A* 68, 063602 (2003).
- <sup>9</sup> A . K uklov and B . S vistonov, *Phys. Rev. Lett.* 90, 100401 (2003); A . K uklov, N . P rokofev, and B . S vistonov, *Phys. Rev. Lett.* 92, 050402 (2004).
- <sup>10</sup> L - M . D uan, E . D em ler, and M . L ukin, *Phys. Rev. Lett.* 91, 090402 (2003).
- <sup>11</sup> A . Isacson, M in - C hui, K . S engupta, and S M . G irvin, *Phys. Rev. B* 72, 184507 (2005).
- <sup>12</sup> M . G reiner, C . A . R egal, and D . S . J in, *Nature* 426, 537-540 (2003).
- <sup>13</sup> M W . Z w ierlein, J R . A bo - S haer, A . S chirotzek, and W . K etterle, *Nature* 435, 1047 (2005).
- <sup>14</sup> For a review, see R . O nofrío and C . P resilla, *J. Stat. Phys.* 115 57 (2004).
- <sup>15</sup> G . R oati, E . de M irandes, F . F erlino, H . O tt, G . M odugno and M . Inguscio, *Phys. Rev. Lett.* 92, 230402 (2004); G . M odugno, E . de M irandes, F . F erlino, H . O tt, G . R oati, and M . Inguscio, *AP Conf. Proc.* 770, 197 (2005).
- <sup>16</sup> R . R oth and K . B umett, *Phys. Rev. A* 69, 021601 (2004).
- <sup>17</sup> A . A lbus, F . I llum unati, and J . E isert, *Phys. Rev. A* 68, 023606 (2003)
- <sup>18</sup> M . L ewenstein, L . S antos, M A . B aranov, and H . F ehmann, *Phys. Rev. Lett.* 92, 050401 (2004).
- <sup>19</sup> M . C ram er, J . E isert, and F . I llum unati, *Phys. Rev. Lett.* 93, 190405 (2004).
- <sup>20</sup> Y . Y u and S . T . C hui, *Phys. Rev. A* 71, 033608 (2005).
- <sup>21</sup> F . I llum unati and A . A lbus, *Phys. Rev. Lett.* 93, 090406 (2004).
- <sup>22</sup> L . D . C arr and M . H olland, *Phys. Rev. A* 72, 031604 (2005).
- <sup>23</sup> More precisely, this means that the Fermions in the mixture is of the same species but can belong to two different total angular momentum (or generalized spin) states<sup>21</sup>.
- <sup>24</sup> S . F lorenz and A . G eorges, *Phys. Rev. B* 70, 035114 (2004); A . G eorges, S . F lorenz, and T . A . C osti, *J. Physique IV* 114, 165 (2004).
- <sup>25</sup> C . S chroll, F . M arquadt, and C . B ruder, *Phys. Rev. A* 70, 053609 (2004).
- <sup>26</sup> J . K . F reericks and H . M onien, *Europhys. Lett.* 26 545 (1994); *ibid Phys. Rev. B* 53 2691 (1996).
- <sup>27</sup> J . S tegner et al, *Nature* 396, 345 (1998).
- <sup>28</sup> J . W idera et al, cond-mat/0505492 (unpublished).
- <sup>29</sup> E . A ltm an, E . D em ler, and M . D . L ukin, *Phys. Rev. A* 70, 013603 (2004).
- <sup>30</sup> M . G reiner, C . A . R egal, J . T . S tewart, and D . S . J in, *Phys. Rev. Lett.* 94, 110401 (2005)
- <sup>31</sup> A . G . T ruscott et al, *Science* 291, 2570 (2004).
- <sup>32</sup> F . S chrek et al, *Phys. Rev. Lett.* 87, 080403 (2001).
- <sup>33</sup> Such a variation also changes  $U_{FF}=U_{BB}$  in principle. But one can achieve an appreciable change in  $\mu$  by maintaining a small change in  $U_{FF}=U_{BB}$  since  $t_F$  has an exponential dependence on the lattice potential.
- <sup>34</sup> G . R oati, F . R iboli, G . M odugno, and M . Inguscio, *Phys. Rev. Lett.* 89, 150403 (2002); F erlino et al, *Phys. rev. A* 73, 040702 (2006).
- <sup>35</sup> The defect state energies are calculated to  $O(t_B^3=U^3)$  in Ref. 26. Here we have only retained terms to  $O(t_B^2=U^2)$  for the purpose of comparison with our approach in Fig. 9 and 10.
- <sup>36</sup> W . K rauth and N . T rivedi, *EuroPhys. Lett.* 14, 627 (1991); W . K rauth, N . T rivedi and D . C eperley, *Phys. Rev. Lett.* 67, 2307 (1991).
- <sup>37</sup> S . S achdev, *Quantum Phase Transitions*, Cambridge University Press, Cambridge, UK (1999).
- <sup>38</sup> B . C aprogrosso-Sansone, N . P rokofev, and B . V . S vistonov, cond-mat/0701178 (unpublished).